Modeling and Validation of Fuel Cell Water Dynamics using Neutron Imaging

Jason B. Siegel, Denise A. McKay, and Anna G. Stefanopoulou

Abstract— Using neutron imaging, the mass of liquid water within the gas diffusion layer and flow channels of an operating polymer electrolyte membrane fuel cell (PEMFC) is measured under a range of operating conditions. Between anode purge events, it is demonstrated that liquid water accumulates and is periodically removed from the anode gas channels; this event is well correlated with the dynamic cell voltage response. The estimation of flooding and cell performance is achieved by a spatially distributed (through-membrane plane), temporally-resolved, and two-phase (liquid and vapor) water model. Neutron imaging techniques have never before been applied to characterize flooding with a dead-ended anode and elucidate important issues in water management as well as provide a means for calibrating and validating a dynamic lumped parameter fuel cell model.

I. INTRODUCTION

The electrochemical power generation of a popular category of fuel cells depends on the proton-conducting properties of their polymer electrolyte membranes. The ability of the membrane to conduct protons increases as water content increases. However, polymer electrolyte membrane fuel cells (PEMFCs) operate below the boiling point of water causing excess water to condense and restrict gas delivery or block the active fuel cell area. The build-up of water mass is referred to as flooding. The impact of flooding is a recoverable reduction in the power output of the fuel cell stack, seen by a decrease in cell voltage [1], [2], but can also lead to irrecoverable material degradation [3]. Thus, a model of the accumulation of liquid water within the PEMFC and its impact on the cell electrical output could facilitate development of a closed-loop observer using cell (or stack) voltage feedback. The estimation can then provide valuable input to diagnostics and control algorithms, including active water management.

Prior work [4], [5], has developed, calibrated and validated a low order model of the liquid water and gas dynamics within the gas diffusion layer (GDL) to simulate both the effects of reactant starvation and flooding for a PEMFC 24-cell stack. By estimating the liquid water wicking out of the gas diffusion layers into the channels, and by relating it to a reduction in the fuel cell active area, the subsequent increase

in the current density was captured and hence the impact of flooding on the electrical output of the cell. Because no direct metric on the accumulation of liquid water within a multi-cell stack was available, the measured cell voltage was compared to the model prediction and the unknown parameters were tuned accordingly.

In this paper neutron imaging is used to measure the mass of liquid water in the gas channels of a single cell. Despite some limitations [6], with careful cell design and masking, the exact location of the liquid water within the cell structure can be inferred, similar to the work of [1], [2], [7], [8], [9], [10]. In addition to image processing, the measured liquid water accumulation in the gas channels is compared to model estimates, and the relationship between cell voltage and the accumulation of liquid water is investigated. Anode versus cathode channel flooding is diagnosed using controlled cathode surging and anode purging events. During a cathode surge, the air flow is momentarily and abruptly increased beyond the nominal excess ratio to remove any liquid water stored in the cathode. During an anode purge, the inlet flow (pure hydrogen) is increased to remove the liquid water stored in the anode. Between these purge events of short duration, the fuel cell system is operated with a dead-ended anode using a pressure regulated supply of dry hydrogen. The operating conditions with a dead-ended anode have never before been observed with neutron imaging, and elucidate important issues in water management. They offer the opportunity to observe the water dynamics during large and repeatable voltage transients and hence provide useful data for calibrating and validating a transient model.

This paper first describes the application of neutron radiography and the experimental methodology used to measure the accumulation of liquid water within the PEMFC channels. Apparent current density as it relates to anode channel flooding is justified. Finally, the estimated liquid water mass and resulting cell voltage is then compared to experimental data.

II. EXPERIMENTAL HARDWARE

The neutron imaging experiments were conducted at the Neutron Imaging Facility at the National Institute for Standards and Technology (NIST) [11]. The amorphous silicon detector was used for its 1Hz image acquisition rate, to capture the change in mass of liquid water over time. Aperture setting 3, and beam 1 were used for the experiment. A NIST test stand was used to supply humidified air to the cathode in flow through operation. A portable anode purging system was constructed, which allows dead-ended operation of the

J.B. Siegel is with the Department of Electrical Engineering and Computer Science, University of Michigan, Ann Arbor, MI 48109 `siegeljb@umich.edu`

D.A. McKay is with the Department of Civil and Environmental Engineering, University of Michigan, Ann Arbor, MI 48109

A.G. Stefanopoulou is with the Department of Mechanical Engineering, University of Michigan, Ann Arbor, MI 48109

fuel cell. This anode purge system consists of a pressure regulator, which supplies dry hydrogen to the anode inlet, and a solenoid valve downstream of the anode outlet. A needle valve placed downstream from the solenoid valve allows the target flow rate during the anode purge to be controlled. Between purges, the anode is supplied with hydrogen via pressure regulation. Table I displays the operating conditions tested at NIST.

TABLE I

CELL OPERATING CONDITIONS

Parameter	Operating Range
Anode inlet RH	0
Cathode inlet RH	40% - 100%
Anode Pressure	123.6 kPa absolute
Cathode Pressure	120-125 kPa absolute
Cell Temperature	40,50,60 ^{o}C
Cell Current	0 - 30 A, 0-566 mA/cm^2

The cell was comprised of a single 53 cm^2, 25.4 μm thick Nafion$^{®}$111-IP membrane. SGL 10BB non-woven carbon gas diffusion layers, were used, which have an uncompressed thickness of 420 μm and a porosity of $\epsilon = 0.84$. The cell hardware, consisted of aluminum endplates, gold coated aluminum current collectors and resin impregnated graphite flow fields [12]. The anode gas channel design was straight and the cathode semi-serpentine. A square 45 W resistive heater, with a surface area of 58 cm^2, was attached to each end plate to ensure uniform heating and maintain desired temperature at low current density.

III. QUANTIFICATION OF LIQUID WATER MASS

Neutron imaging is a useful tool for in-situ measurement of liquid water in fuel cell systems. The attenuation properties of a neutron beam passing through an object can be used to form a projected image on a detector, similar to X-ray radiography. Neutrons are strongly scattered by hydrogen atoms, which are concentrated in liquid water within the fuel cell, and only weakly interact with other materials used in PEMFCs, such as aluminum and carbon. Therefore, neutron images are very sensitive to the amount of liquid water present in the cell.

Fig. 1 shows two water thickness images collected during testing at NIST. The areas with high liquid water accumulation are clearly visible in the top left picture, which corresponds to a condition before an anode purge event. The second frame in Fig. 1 shows the drier neutron image collected after an anode purge that significantly improved the voltage response of the cell.

The image formed by scattering and absorption of neutrons can be modelled by the Beer-Lambert law. The relative neutron transmission, which is found by dividing an image with the reference image of the fuel cell, can be used to calculate water thickness, assuming that the attenuation caused by everything else in the cell remains the same since the reference image was captured. To reduce systematic error, care was taken to ensure reference images were taken of a

Before Anode Purge

Following Anode Purge

0 mm *2 mm*
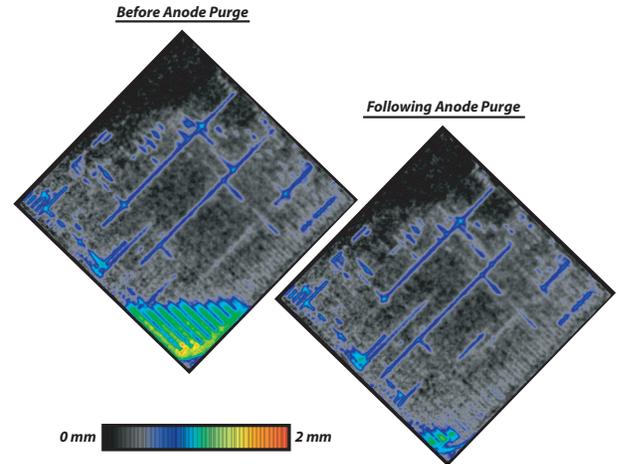
Fig. 1. Masked neutron images of the fuel cell before and after anode purge events. The cell was operated at 566 mA/cm^2, 55°C, and an air stoichiometry of 200% with a fully humidified cathode supply gas.

completely dry cell. The thickness of the water layer,

$$t_w(j,k) = -\frac{1}{\mu_w} \ln \left[\frac{I^{norm}(j,k)}{I^{norm}_{dry}(j,k)} \right] , \qquad (1)$$

is calculated from the images using the experimentally obtained attenuation coefficient (μ_w=0.3708 $\pm$0.0008 mm^{-1}) from [11]. A 3x3 median filter is applied to the images to remove noise.

A. Masking

The processed water thickness image, $t_w(j,k)$, is a 2-D projection of the liquid water content inside the fuel cell. To infer the location of liquid water in the third dimension, knowledge of the physical material structure can be combined with logical arguments; for example, liquid water cannot be located within an impervious solid material. Several masking techniques have been used to analyze neutron images [9], [1], [10], [2]. A similar process is employed here to estimate the mass of liquid water in three layers: the anode channel, cathode channel and combined membrane and GDL layer (which consists of both anode and cathode GDLs). Four mutually disjoint masks, D-G, identify regions of the fuel cell corresponding to the different possible combinations of channels and lands on each side of the membrane as shown in Fig. (2). The area of each mask, and its relationships to other masks are shown in Table II. The water thickness in the combined membrane and GDL layer can be directly measured from the images for regions identified by mask G, which contains lands on both sides, and therefore, the water can not be present in either of the other two layers. A fifth mask, H, which is a subset of the area under both anode and cathode lands, is used get a more accurate estimate of the water content in the combined GDL / Membrane layer. Mask H chooses points in the center of mask G, away from the channel, reducing possible effects of instrument broadening when liquid water is present in the channels [7], [11].
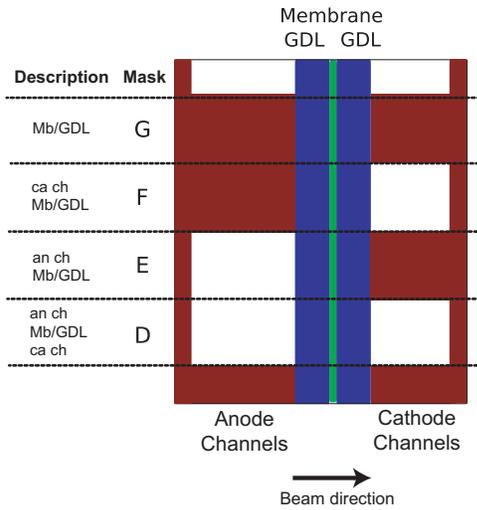
Fig. 2.   Schematic of fuel cell layers

TABLE II
MASKS

Mask	Description	#Pixels	Relationship
A	Active Area	313600	$D \cup E \cup F \cup G$
B	Anode Channel Area	234099	
C	Cathode Channel Area	169392	
D	Both Ch +MEMB+GDL	128047	$B \cap C$
E	An Ch + MEMB+GDL	106052	$(B \cap \bar{C}) \cap A$
F	Ca Ch + MEMB+GDL	41345	$(\bar{B} \cap C) \cap A$
G	MEMB+GDL only	38155	$(\bar{B} \cap \bar{C}) \cap A$
H	Subset of G	11239	$H \subset G$

B. Spatial (2-D) Averaging

Using masking, the gradients in the liquid water concentration along the channels are checked to determine if they limit the application of 2-D spatial averaging to calculate the distribution of liquid water in the third dimension. Specifically, the active area is also partitioned into a 9x9 grid similar to [2]. The fuel cell conditions are assumed to be uniform in each of the 81 segments. Five image masks (D-H) are applied to each of the 81 segments individually, and the average liquid water thickness in each masked regions is calculated for each segment.

If it is assumed that the liquid water thickness in the combined membrane and GDL layers is uniform over the entire segment, then it must equal to the averaged thickness in the region defined by mask H for that segment. The average liquid water thickness in the anode channel can be estimated by the difference between averaged water thickness in masked regions H and E, since no cathode water is possible in either region. Similarly, average cathode channel liquid water thickness can be estimated by the difference between averaged water thickness in regions H and F, assuming that any water thickness beyond that measured in the masked area H, must reside in the channel. The calculated average water thickness in each segment for each of the three layers - anode channel, combined membrane/GDL and cathode channel - can be converted to the mass in grams by multiplying by

the area in each masks B, A, or C respectively for the given segment and dividing by the density of water. The total liquid water mass in the cell is found by summing the masses calculated for each of the 81 segments.

The percent difference between the total liquid water mass and the sum of the estimated masses calculated via masked local averages is less than 2%. The relative uncertainty introduced by the assumption of a uniform water thickness in the combined membrane and GDL layer for each segment is small, Therefore we have a high level of confidence using the locally averaged and masked data to infer the mass of liquid water in each of the three layers.

IV. CHANNEL FLOODING AND VOLTAGE CORRELATION

The neutron imaging data, with the applied masking techniques, confirms the presence of liquid water in the anode channel, as shown in Fig. 3 for a typical purge cycle. Following an anode purge, all of the liquid water in the anode channel is removed, then slowly accumulates until the next purge event. This buildup of liquid water in the anode channel, as well as the GDL and membrane, is well correlated with the observed recoverable voltage degradation, up to 100 mV, between purges. Note, there is little change in the cathode channel water mass between or during purges.
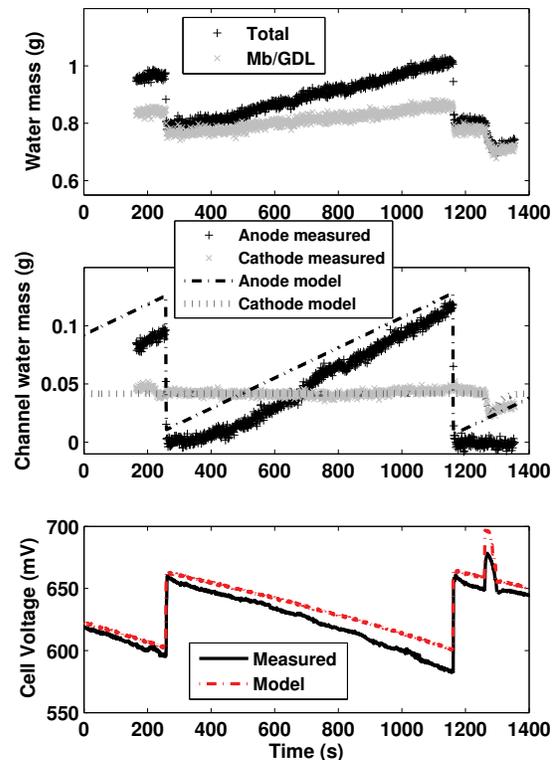
Fig. 3.   Measured cell voltage degradation and liquid water mass accumulation between anode purges. These experiments were conducted with fully humidified air at a current density of 378 mA/cm^2, a cell operating temperature of 50°C, and an air stoichiometry of 300%.

Following the anode purge, a cathode surge was conducted at approximately 1300 seconds. During these dynamics, the mass of liquid water in the cathode channel decreases as a result of the increased water removal rate with higher flow. The cell voltage increases due to the higher oxygen partial pressure. After the cathode flow rate is restored, the voltage returns to its previous value. In some experiments, even when the cathode surge event occurs prior to the anode purge event, the voltage will continue to degrade at the same rate as experienced previous to the cathode surge. These results indicate that liquid water in cathode channel has little effect on voltage under these conditions. In contrast, following the two anode purges at 250 and 1150 seconds, the voltage recovery is significant and sustained until liquid water begins to accumulate in the anode channel again.

Different operating conditions exist such that cathode, rather than anode, flooding is the predominate cause of voltage degradation. During these conditions, a sustained recovery in voltage and a clear decrease in cathode channel liquid water mass is observed, while anode channel liquid water mass is constant and not impacted by purge events. As a result, cathode surges and anode purges can be used as a diagnostic tool to determine the presence of liquid water in each channel volume by characterizing the voltage response.

A. Apparent Current Density

Once anode flooding occurs, the resulting voltage degradation is associated with the accumulation of liquid water mass in the anode channel, $m_{l,an,ch}$, which is assumed to form a thin film of thickness, t_{wl}, blocking part of the active fuel cell area, A_{fc}, and consequently increasing the apparent current density, i_{app} in A/cm^2,

$$i_{app} = \frac{I_{st}}{10000 A_{app}}, \tag{2}$$

where the apparent fuel cell area, A_{app} in m^2, is approximated as

$$A_{app} = A_{fc} - \frac{1.3 \, m_{l,an,ch}}{n_{cells} \, \rho_l \, t_{wl}}, \tag{3}$$

using a scaling factor of 1.3 as the ratio of the total active area to the anode channel area. The thickness of this water layer, t_{wl} is a tunable parameter that impacts the rate of voltage decay as liquid water accumulates.

The cell voltage,

$$v = E - U_{act} - U_{ohmic} \tag{4}$$

accounts for the theoretical open circuit voltage,

$$E = -\left(\frac{\Delta H}{2F} - \frac{T \Delta S}{2F}\right) + \frac{RT}{2F} ln\left(\frac{p_{H_2,an,mb}\sqrt{p_{O_2,ca,mb}}}{(p_o)^{1.5}}\right) \tag{5}$$

the total activation voltage loss [13],

$$U_{act} = K_1 \frac{RT}{F} \ln\left(\frac{i_{app}}{i_o}\right), \tag{6}$$

the exchange current density,

$$i_0 = K_2 \left(\frac{p_{O_2,ca,mb}}{p_o}\right)^{K_3} \exp\left[-\frac{E_c}{RT}\left(1 - \frac{T}{T_o}\right)\right], \tag{7}$$

and the ohmic voltage loss [14],

$$U_{ohmic} = K_4 \left[\frac{t_{mb}}{(b_{11}\lambda_{mb} - b_{12})} e^{-1268\left(\frac{1}{303} - \frac{1}{T}\right)}\right] i_{app}, \tag{8}$$

where ΔS and ΔH are the differences in entropy and enthalpy from standard state conditions, p_o is the standard pressure, $p_{O_2,ca,mb}$ and $p_{H_2,an,mb}$ are the oxygen and hydrogen partial pressures at the GDL-membrane interface, K_1-K_4 are tunable parameters, E_c is the activation energy for oxygen reduction on Pt, T_o is the reference temperature, t_{mb} is the membrane thickness, b_{11} and b_{12} are experimentally identified parameters from [14], and λ_{mb} is the membrane water content.

B. Channel and GDL Dynamics

The predicted anode and cathode channel masses are compared to the measured values in Fig. 3. The predicted water accumulation in the channels depends on the water flow (both vapor and liquid) from the GDL. The reactant and water dynamics in a GDL are briefly described here and detailed in [4], [5]. The hydrogen and water vapor concentration are expressed as

$$\frac{\partial c_{H_2}}{\partial t} = -\frac{\partial}{\partial y}\left(\langle D_{H_2}\rangle \frac{\partial c_{H_2}}{\partial y}\right), \tag{9a}$$

$$\frac{\partial c_v}{\partial t} = -\frac{\partial}{\partial y}\left(\langle D_v\rangle \frac{\partial c_v}{\partial y} + R_{evap}\right), \tag{9b}$$

where the molar evaporation rate is $R_{evap} = \gamma \frac{p_{sat}-p_v}{RT}$, and the effective diffusivity of the gas constituents in the GDL are a function of liquid water saturation, $s = \frac{V_l}{V_p}$,

$$\langle D_j\rangle = D_j\epsilon \left(\frac{\epsilon - 0.11}{1 - 0.11}\right)^{0.785} (1 - s)^2. \tag{10}$$

Similarly, these equations are employed on the cathode for oxygen, water vapor and nitrogen.

Applying conservation of mass to the liquid water in the GDL, using ρ_l for liquid water density, M_v for molecular weight of water, ϵ for GDL porosity, K for GDL permeability, μ_l for liquid water viscosity, θ_c for contact angle, and σ for surface tension,

$$\frac{\partial s}{\partial t} = \frac{K \, S^3}{\mu_l} \frac{\partial}{\partial y}\left[\left(\frac{\partial p_c}{\partial S}\right)\left(\frac{\partial S}{\partial y}\right)\right] - \frac{R_{evap}M_v}{\rho_l}, \tag{11}$$

where the liquid water capillary pressure is expressed as

$$p_c = \frac{\sigma \cos\theta_c}{\sqrt{K/\epsilon}}[1.417S - 2.120S^2 + 1.263S^3], \tag{12}$$

with S being the reduced liquid water saturation,

$$S = \begin{cases} \frac{s - s_{im}}{1 - s_{im}} & \text{for} \quad s_{im} < s \leq 1 \\ 0 & \text{for} \quad 0 \leq s \leq s_{im} \end{cases} \tag{13}$$

which is used to model the interruption of capillary flow when the water saturation falls below the immobile saturation limit, s_{im}.

The membrane and gas channels serve as time-varying boundary conditions for the GDL model. Water vapor is

exchanged between the anode and cathode at the membrane and generated at the cathode due to the chemical reaction, implying that the fluxes of all gaseous constituents in the membrane boundary are calculated based on the reaction rates and the membrane water transport. At the GDL-channel interface, the liquid water saturation is set equal to the immobile saturation, $s \mid_{y=L} = s_{im}$, and it is assumed no liquid water is transported through the membrane $\frac{\partial S}{\partial y} \mid_{y=0} = 0$. Mass conservation is applied to the channels to specify the channel gas concentration boundary conditions.

The model described in [4], [5] is modified to include liquid water removal from the channel, which is proportional to total gas flow rate [15], and the mass of liquid water, to prohibit a flow of liquid water when no liquid water is present in the channel, such that

$$W_{l,ch,out} = k_{l,ch,out} \, m_{l,ch} W_{gas,ch,out}. \qquad (14)$$

V. MODEL VALIDATION

The model is tuned based on a whole day experiment. The tunable parameters consist of the four tuning parameters in the voltage model $(K_1 - K_4)$, the water thickness layer in the anode channel t_{wl} which affects the apparent current density, and a scaling factor α_{Dw} which tunes the membrane water transport as detailed in [5]. The addition of liquid water removal is needed to model the channel water mass, but requires the tuning of two additional parameters $k_{l,an,ch}$ and $k_{l,an,ch}$. First α_{Dw}, $k_{l,an,out}$ and $k_{l,ca,out}$ are chosen, via simulation, to match the rate of change of liquid water in the anode and cathode channels. Once these values have been optimized, the four voltage parameters can be tuned using a linear least squares approach based on the error between the predicted voltage and measurement, for a given value of t_{wl}. The voltage error for several reasonable values of t_{wl} are then calculated and the optimum is chosen graphically. In summary, 3 parameters can be chosen using an on-line optimization via simulating the model. The remaining 5 parameters can be optimized off-line since they are used in the voltage model which defines the output of the system.

The measured and estimated liquid water channel masses were then compared under a wide range of operating conditions consisting of seven hours of continuous testing, as shown in Fig. 4. During this experiment, the cell was operated with changes in cathode flow corresponding to oxygen excess ratio (fraction of air supplied divided by the air necessary for the reaction rate) of λ=2-3, and stack current densities of i=190-570 mA/cm^2. The cell temperature and cathode relative humidity were held constant, at 40°C and 70%, for the first two thirds of the data, then both were increased to 50°C and fully humidified for the remainder of the data set. Image data were not collected continuously, which accounts for gaps in the measured liquid water mass data. The cell was operated through several anode purge cycles while holding the PEMFC operating conditions steady until the voltage responses were repeatable and then neutron image acquisition was initiated. Other image data were also taken during transients such as load changes.

Using the notion of apparent current density to relate the accumulated mass of liquid water in the anode channel to the resulting voltage degradation, the model prediction of voltage agrees well with the measured value between purges as well as during purging and surging events. Fast voltage responses due to the increase in oxygen partial pressure during surges are also estimated well because of the inclusion of the fast reactant dynamics associated with gas concentrations. The model predicts that all of the liquid water mass is removed from the anode channel following a purge. Although the model does not precisely estimate the cathode channel mass, the general trend is acceptable.

At lower current density, 189 mA cm^{-2}, the liquid water accumulation in the anode channels was distributed throughout the entire active area, which suggests that the anode gas flow rate at low current density is not sufficient to push water to the end of the cell where it can be removed by purging. This is seen in the buildup of liquid water mass in the anode channel Fig. 4 between 120-150 min, which is insensitive to anode purges. The liquid water in the anode channel does not continue to increase during this period, but voltage degradation is observed which responds to anode purging. This suggests that another factor such as nitrogen accumulation in the anode, which is still cleared by the purge, may contribute to the voltage drop [16].

Between approximately 170-270 minutes, several pressure disturbances occurred that impacted the air delivery system supplied to the test bench. These disturbances caused a significant drop in cell voltage due to poorly regulated air delivery to the cell, but did not prevent the model from accurately predicting the slower dynamics of flooding.

VI. CONCLUSIONS AND FUTURE WORK

The model predicts anode flooding in a PEMFC with dead-ended anode for a wide range of conditions, and for approximately 80% of the testing time. The model can be used for control purposes, such as optimizing the purge interval and duration for minimal H$_2$ waste, by scheduling the purge events utilizing voltage measurements as feedback instead of over-conservative feedforward schemes. The model can easily be modified to represent flow through conditions for anode fuel delivery. In this case, the stoichiometric ratio and inlet relative humidity might be adjusted to optimized fuel cell efficiency.

Upon examination of other operating conditions during four days of testing (42 hours), the model does not accurately predict the mass of liquid water at low cathode inlet relative humidity (50%) or at low cathode flow rates (which occur at low current density and/or low air stoichiometry). At low current density more water is retained in the cell, as seen in the neutron imaging, since the gas velocity in the channel is smaller and less liquid water is removed from the channel with the excess gas flow. A more in-depth study of liquid water removal by the cathode gas stream should yield improvement in the model prediction under these conditions. The addition of cathode catalyst layer flooding is necessary for higher current density operation, and modeling nitrogen
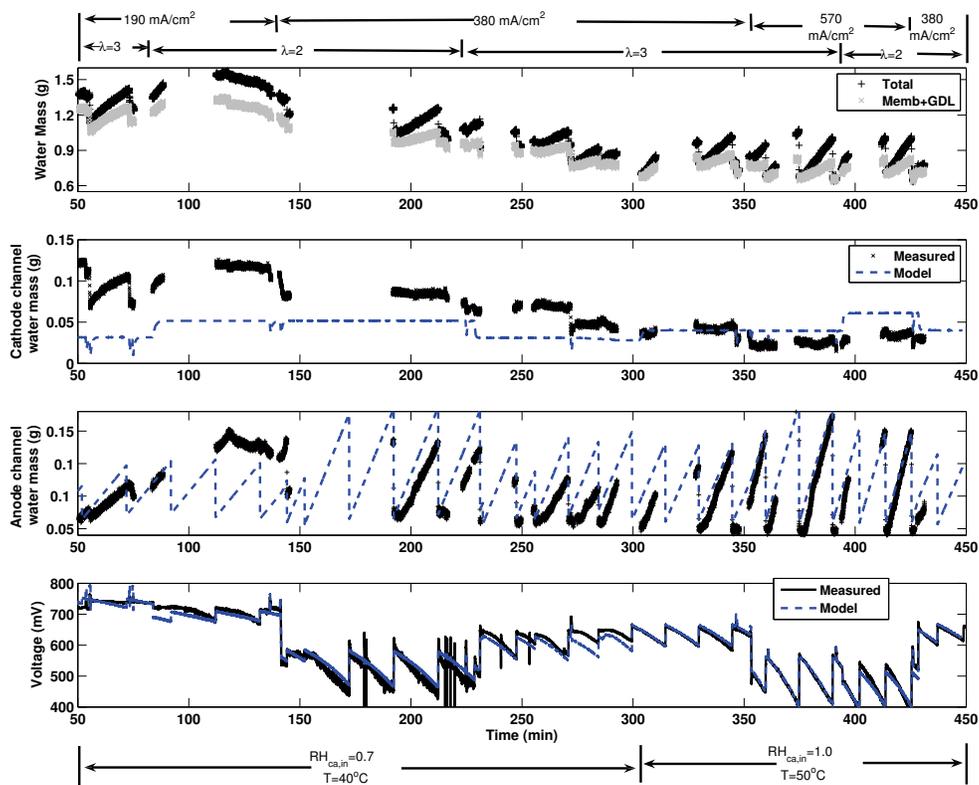
Fig. 4.   Comparison of estimated and measured liquid water mass and the resulting prediction of voltage.

accumulation in the anode of dead-ended cells should also improve model fidelity. Sensitivity and identifiability of both tuned and non-tuned parameters in the model such as, evaporation rate γ, immobile saturation limit s_{im} and the functional form of the boundary conditions are currently under investigation.

REFERENCES

[1] P. A. Chuang, A. Turhan, A. K. Heller, J. S. Brenizer, T. A. Trabold, and M. M. Mench, "THE NATURE OF FLOODING AND DRYING IN POLYMER ELECTROLYTE FUEL CELLS," in *Third International Conference on Fuel Cell Science, Engineering and Technology*, 2005.
[2] Y.-S. Chen, H. Peng, D. S. Hussey, D. L. Jacobson, D. T. Tran, T. Abdel-Baset, and M. Biernacki, "Water distribution measurement for a PEMFC through neutron radiography," *Journal of Power Sources*, vol. 170, no. 2, pp. 376–386, July 2007.
[3] J. St-Pierre, D. P. Wilkinson, S. Knights, and M. Bos, "Relationships between water management, contamination and lifetime degradation in PEFC," *Journal of New materials for Electrochemical Systems*, vol. 3, pp. 99–106, 2000.
[4] D. A. McKay, W. T. Ott, and A. Stefanopoulou, "Modeling, Parameter Identification, and Validation of Water Dynamics for a Fuel Cell Stack," in *Proceedings of 2005 ASME International Mechanical Engineering Congress & Exposition*, vol. IMECE 2005-81484, Nov 2005.
[5] D. A. McKay, J. B. Siegel, W. Ott, and A. G. Stefanopoulou, "Parameterization and Prediction of Temporal Fuel Cell Voltage Behavior During Flooding and Drying Conditions," *Journal of Power Sources*, vol. 178, pp. 207–222, March 2008.
[6] H. Ju, G. Luo, and C.-Y. Wang, "Probing Liquid Water Saturation in Diffusion Media of Polymer Electrolyte Fuel Cells," *Journal of the Electrochemical Society*, vol. 154, no. 2, pp. B218–B228, Feb. 2007.

[7] D. Kramer, J. Zhang, R. Shimoi, E. Lehmann, A. Wokaun, K. Shinohara, and G. Scherer, "In situ diagnostic of two-phase flow phenomena in polymer electrolyte fuel cells by neturon imaging Part A. Experimental, data treatment, and quantification," *Electrochimica Acta*, vol. 50, pp. 2603–2614, 2005.
[8] T. Trabold, J. Owejan, D. Jacobsen, M. Arif, and P. Huffman, "In Situ Investigation of Water Transport in an Operating PEM Fuel Cell Using Neutron Radiography: Part I-Experimental Method and Serpentine Flow Field Results," *International Journal of Heat and Mass Transfer*, vol. 49, pp. 4712–4720, 2006.
[9] R. Satija, D. L. Jacobson, M. Arif, and S. A. Werner, "In situ neutron imaging technique for evaluation of water management systems in operating PEM fuel cells," *Journal of Power Sources*, vol. 129, no. 2, pp. 238–245, Apr. 2004.
[10] A. Turhan, K. Heller, J. Brenizer, and M. Mench, "Quantification of liquid water accumulation and distribution in a polymer electrolyte fuel cell using neutron imaging," *Journal of Power Sources*, vol. 160, pp. 1195–1203, 2006.
[11] D. Hussey, D. Jacobson, and M. Arif, "In situ fuel cell water metrology at the NIST neutron imaging facility," *Proceedings of the ASME International Conference on Fuel Cell Science, Engineering and Technology*, 2007.
[12] M. Hickner, N. Siegel, K. Chen, D. McBrayer, D. Hussey, D. Jacobson, and M. Arif, "Real-Time Imaging of Liquid Water in an Operating Proton Exchange Membrane Fuel Cell," *Journal of the Electrochemical Society*, vol. 153, pp. A902–A908, 2006.
[13] F. Barbir, *PEM Fuel Cells: Theory and Practice*. Burlington, Ma: Elsevier, 2005.
[14] T. Springer, T. Zawodzinski, and S. Gottesfeld, "Polymer Electrolyte Fuel Cell Model," *Journal of the Electrochemical Society*, vol. 138, no. 8, 1991.
[15] E. Kumbur, K. Sharp, and M. Mench, "Liquid droplet behavior and instability in a polymer electrolyte fuel cell flow channel," *Journal of Power Sources*, vol. 161, no. 1, pp. 333–345, Oct. 2006.
[16] E. A. Muller, F. Klob, L. Guzzella, and A. Stefanopoulou, "Correlating Nitrogen Accumulation with Temporal Fuel Cell Performance," *submitted to ASME DCSS*, 2008.